Electrical resistance of Moiré pattern hexagonal lattices

February 11, 2021

1 Introduction

When the layers in bilayer graphene are twisted at the *magic angle* ($\approx 1.1°$) and are conditioned at temperatures below 1.7 K, the material becomes a superconductor, where electrons can be transported with no electrical resistance.[1] This discovery has directly influenced the forming of the field of *twistronics* (twist-electronics), which aims to quantify how the twist between the layers of 2d-materials affects their electronic properties.[2]

Graphene is an allotrope of carbon, where each carbon atom is connected to 3 others by covalent bonds, forming a 2d sheet. As such, graphene can be represented by a hexagonal lattice, with its vertices representing carbon atoms and edges representing the bonds. Twisted bilayer graphene on the other hand forms a hexagonal Moiré pattern like that in Fig. 1, causing larger hexagonal cells to be formed and a corresponding hexagonal *super-structure*.

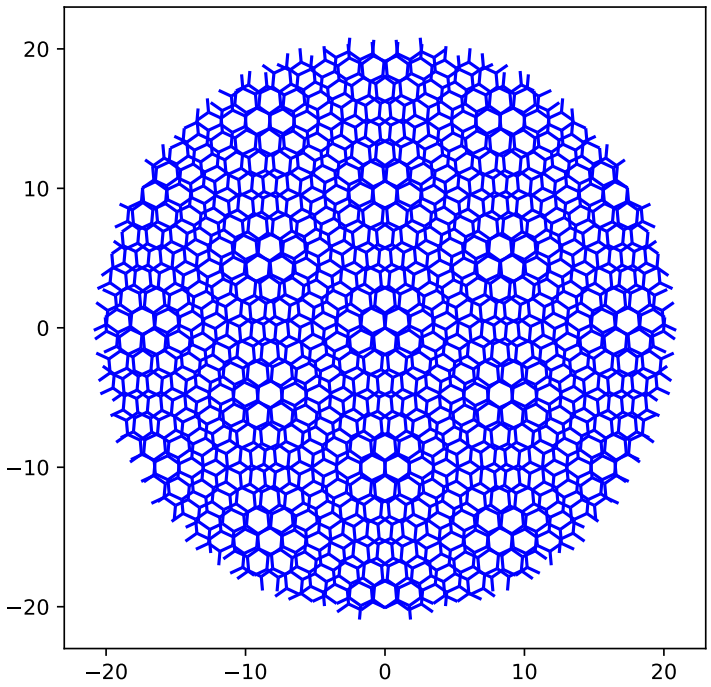

Figure 1: Hexagonal Moiré pattern formed by an angle of twist $\theta = 10°$, $R = 20$

Explaining and quantifying the superconductivity of these structures has been the subject of research of many physicists. So in an attempt to explain the magic angle myself,

I decided to approach this phenomena with what I had learnt about electronic circuits so far—Kirchoff's Circuit Law. Hence, the research question of this investigation is: Can twisted bilayer graphene's superconductivity at the magic angle be explained using an Ohmic-model of resistance? Since it is impossible to have $0\,\Omega$ resistance within the Ohmic model without a short circuit, the goal is to determine whether the resistance at the magic angle is the global minimum of the resistance vs angle graph of the Moiré lattice.

2 Research Method

A completely computational method had to be used due to lack of access to a 3d-printer with conductive filaments to perform physical experiments. Moreover, since existing simulation software such as SPICE[3] were not meant for geometrically constructed circuits, I created my own software, featuring Moiré lattice generation methods and line intersection algorithms to obtain circuit nodes, they are omitted here because they are beyond the scope of this essay.

There are no ethical or safety hazards to consider due to the computational nature of this investigation.

2.1 Problem Definition

For the sake of consistency, each hexagonal cell within the Moiré lattice has a side length of one (unitless) and the center of the lattice at coordinate $(0, 0)$ has a shape resembling shape (Λ) instead of ($\hexagon$). Each edge has an electrical resistance equal to the magnitude of its length Ohms, for example a segment of length 1 has resistance $1\,\Omega$. Let the size of the lattice be bounded by a circle with radius R, meaning that all the outermost edges will intersect this circle.

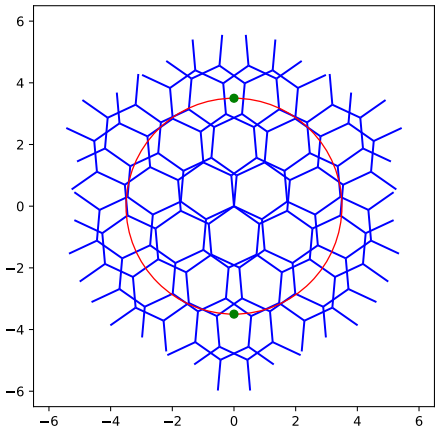

Figure 2: Hexagonal Moiré pattern with reference circle (red) and reference points (green), $R = 5$, $r = 3.5$, $\theta = 10°$

In order to answer the research question, the electrical resistance between 2 *reference* points must be measured. These points are defined as having the coordinates $(0, r)$ and $(0, -r)$ *for all* angles of twist θ between 2 hexagonal lattice layers.

There are 2 methods to form bilayer grids with twist θ as shown in Fig. 3a and Fig. 3b. Fig. 3a is chosen because it preserves vertical symmetry, allowing the relative positions

of the reference points against the 2 lattices to be identical (except for the reflection transformation).

(a) (b)

Figure 3: Twisting 2 layers by θ

Also, the fixed definition of the reference points allows their positions to be invariant to θ. Since these reference points are not necessarily on the Moiré grid, i.e., $(0, r)$ may not be on a lattice edge, a *reference circle* is employed. The reference circle has radius r and is centered at $(0, 0)$ like that in Fig. 2. Note that the circle is part of the circuit, forming its own edges and electrical connections, allowing for the reference points to connect with the rest of the hexagonal lattice. Although the circle is not part of graphene's structure, the overall effect the circle has on the resistance between the 2 reference points diminishes with increasing r, because the ratio of the number of paths on the circumference of the reference circle to the paths within the reference circle $\propto \frac{r}{r^2}$. Simply put, the hexagonal lattice within the reference circle influences the resistance more than the reference circle.

After the reference points, reference circle, and 2 hexagonal lattices are generated, the intersections between all of them are calculated in order to create *nodes*, additional vertices within the circuit which are created by overlapping line segments (i.e., electrical wires). Instead of the circular arcs depicted like that in Fig. 2, each segment within the reference circle is modelled using 2 straight line segments Fig. 5, whose total length matches the length of the circular arc—the circular arc and the straight line segments are electrically equivalent. The reference points are placed atop this "circle".

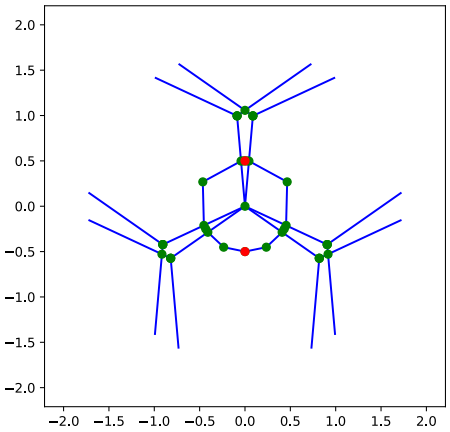

Figure 4: Nodes within a lattice of overlapping hexagonal grids and a reference circle, with nodes (green), reference points (red), $R = 1.1$, $r = 0.5$, $\theta = 10°$

2.2 Nodal analysis

In order to find the resistance between these two reference points, a fixed amount of current (i.e., 1 A) is "injected" into one reference point and extracted from the other reference point. The resulting voltage difference between them can be used to calculate the effective resistance between these points, which is taken to be the effective resistance of the Moiré lattice. The following descriptions outline a method based on [4] to compute these voltages given the resistance between all nodes (calculated through the coordinates of these nodes, since length is assumed to be synonymous with resistance).

2.2.1 Kirchoff's Circuit Law

Kirchoff's Current Law (KCL) states that the net current—the sum between ingoing and outgoing currents—of any node is zero, *unless there is an external current source.*

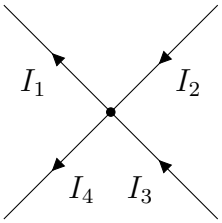

Figure 5: Applying KCL yields $I_1 + I_4 = I_2 + I_3$

KCL can be represented mathematically through the equation

$$\sum_{i \neq j} I_{i,j} = 0\,\text{A} \tag{1}$$

where $I_{i,j}$ indicates the current from node i "flowing" into node j. $R_{i,j}$ represents the resistance between the nodes. Note that i and j should are directly connected through a single edge (i.e., no nodes in between). If nodes i and j are not directly connected, then $I_{i,j} = 0\,\text{A}$ and $R_{i,j} = \infty\,\Omega$.

2.2.2 Ohm's Law

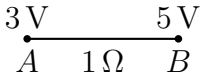

Figure 6: Simple circuit with $V_A = 3\,\text{V}$, $V_B = 5\,\text{V}$, and $R_{A,B} = 1\,\Omega$

Ohm's law states that $V = IR$. Taking Fig. 6 as an example, a more precise definition of $I_{i,j}$ using nodes can be stated as

$$\begin{aligned} I_{i,j} &= \frac{V_i - V_j}{R_{i,j}} \\ &= \frac{V_i}{R_{i,j}} - \frac{V_j}{R_{i,j}} \\ I_{A,B} &= -2\,\text{A} \end{aligned} \tag{2}$$

Note that $I_{i,j}$ is signed.

With $G_{i,j} = R_{i,j}^{-1}$ representing conductance, combining Eq. 1 and Eq. 2 yields

$$\begin{aligned}\sum_{i \neq j} I_{i,j} &= \sum_{i \neq j} \frac{1}{R_{i,j}}(V_i - V_j) \\ &= \sum_{i \neq j} G_{i,j} V_i - \sum_{i \neq j} G_{i,j} V_j \\ &= 0\,\text{A}\end{aligned} \tag{3}$$

Eq. 3 forms the basis of node-voltage analysis. It can be used construct the linear system

$$\mathbf{G}\mathbf{V} = \mathbf{I} \tag{4}$$

where $\mathbf{G}$, $\mathbf{V}$, and $\mathbf{I}$ is the conductance matrix, voltage vector, and current vector, with dimensions $N \times N$, $N \times 1$, and $N \times 1$ respectively with N as the total number of nodes in the lattice. $\mathbf{V}_i$ represents the voltage of node i and $\mathbf{I}_i$ represents the net current of node i, which is typically 0, unless i is a reference node in which case $\mathbf{I}_i = \pm 1\,\text{A}$—one reference point has net current $1\,\text{A}$, while the other has net current $-1\,\text{A}$ in order to obey the law of charge conservation. $\mathbf{G}$ on the other hand is defined as

$$\mathbf{G}_{i,j} = \begin{cases} \sum_{i \neq k} G_{i,k} & \text{if } i = j\text{, sum of all conductances connected to } i \\ -G_{i,j} & \text{if } i \neq j \end{cases} \tag{5}$$

Eq. 4 can be proved by performing a dot product between a row in $\mathbf{G}$ and $\mathbf{V}$. Take for example the first row of $\mathbf{G}$,

$$\begin{aligned}\mathbf{I}_1 &= \mathbf{G}_{1,1}\mathbf{V}_1 + \mathbf{G}_{1,2}\mathbf{V}_1 + \mathbf{G}_{1,3}\mathbf{V}_3 + ... \\ &= \sum_{1 \neq k} G_{1,k}\mathbf{V}_1 - G_{1,2}\mathbf{V}_2 - G_{1,3}\mathbf{V}_3 - ... \\ &= \sum_{1 \neq k} G_{1,k}\mathbf{V}_1 - \sum_{1 \neq j} G_{1,j}\mathbf{V}_j\end{aligned} \tag{6}$$

Therefore, Eq. 6 and Eq. 3 are equivalent.

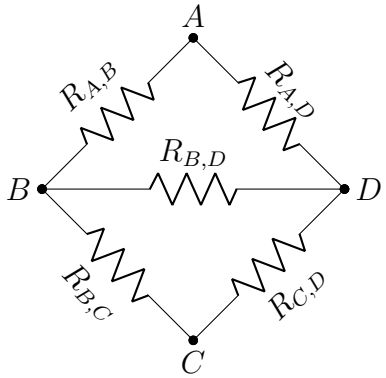

Figure 7: Wheatstone bridge, with $R_{A,B} = 2\,\Omega$, $R_{A,D} = 3\,\Omega$, $R_{B,D} = 6\,\Omega$, $R_{B,C} = 4\,\Omega$, and $R_{C,D} = 5\,\Omega$

Take for example the Wheatstone bridge in Fig. 7. Let A and C be reference points, then Eq. 4 can be expanded as:

$$\mathbf{GV} = \mathbf{I}$$

$$\begin{array}{c} \\ A \\ B \\ C \\ D \end{array} \begin{array}{c} \begin{array}{cccc} A & B & C & D \end{array} \\ \begin{bmatrix} \frac{5}{6} & -\frac{1}{2} & 0 & -\frac{1}{3} \\ -\frac{1}{2} & \frac{11}{12} & -\frac{1}{4} & -\frac{1}{6} \\ 0 & -\frac{1}{4} & \frac{9}{20} & -\frac{1}{5} \\ -\frac{1}{3} & -\frac{1}{6} & -\frac{1}{5} & \frac{7}{10} \end{bmatrix} \end{array} \begin{bmatrix} \mathbf{V}_A \\ \mathbf{V}_B \\ \mathbf{V}_C \\ \mathbf{V}_D \end{bmatrix} = \begin{bmatrix} 1 \\ 0 \\ -1 \\ 0 \end{bmatrix} \tag{7}$$

To find $\mathbf{V}$, the linear system can be inverted, forming

$$\begin{aligned} \mathbf{GV} &= \mathbf{I} \\ \mathbf{G}^{-1}\mathbf{GV} &= \mathbf{G}^{-1}\mathbf{I} \\ \mathbf{V} &= \mathbf{G}^{-1}\mathbf{I} \end{aligned} \tag{8}$$

However, $\mathbf{G}$ is singular. Intuitively, this is because any voltage reference (i.e., where $V = 0\,\mathrm{V}$) can be chosen. For simplicity's sake, $\mathbf{V}_D$ will be chosen as the voltage reference. Now the last column and row of $\mathbf{G}$ can be omitted entirely and matrix inversion can be applied.

$$\begin{aligned} \mathbf{V} &= \mathbf{G}^{-1}\mathbf{I} \\ \begin{bmatrix} \mathbf{V}_A \\ \mathbf{V}_B \\ \mathbf{V}_C \end{bmatrix} &= \begin{bmatrix} \frac{5}{6} & -\frac{1}{2} & 0 \\ -\frac{1}{2} & \frac{11}{12} & -\frac{1}{4} \\ 0 & -\frac{1}{4} & \frac{9}{20} \end{bmatrix}^{-1} \begin{bmatrix} 1 \\ 0 \\ -1 \end{bmatrix} \\ &= \begin{bmatrix} \frac{84}{43} & \frac{54}{43} & \frac{30}{43} \\ \frac{54}{43} & \frac{90}{43} & \frac{50}{43} \\ \frac{30}{43} & \frac{50}{43} & \frac{370}{129} \end{bmatrix} \begin{bmatrix} 1 \\ 0 \\ -1 \end{bmatrix} \\ &= \begin{bmatrix} \frac{54}{43} \\ \frac{4}{43} \\ -\frac{280}{129} \end{bmatrix} \approx \begin{bmatrix} 1.26 \\ 0.09 \\ -2.17 \end{bmatrix} \end{aligned} \tag{9}$$

Finally, the effective resistance between nodes A and C can be determined to be $R_e = |\frac{\Delta V}{I}| = \frac{442}{129} \approx 3.43\,\Omega$.

3 Results

The nodal analysis method used within the Wheatstone bridge example was used to calculate the resistance in hexagonal Moiré patterns. In particular, a lattice parameterized by $R = 30$, $r = 15$, and various angles of θ (360 calculations, one for each degree between $0°$ and $360°$) was chosen. Due to the sheer number of nodes involved (> 16000), matrices will not be shown.

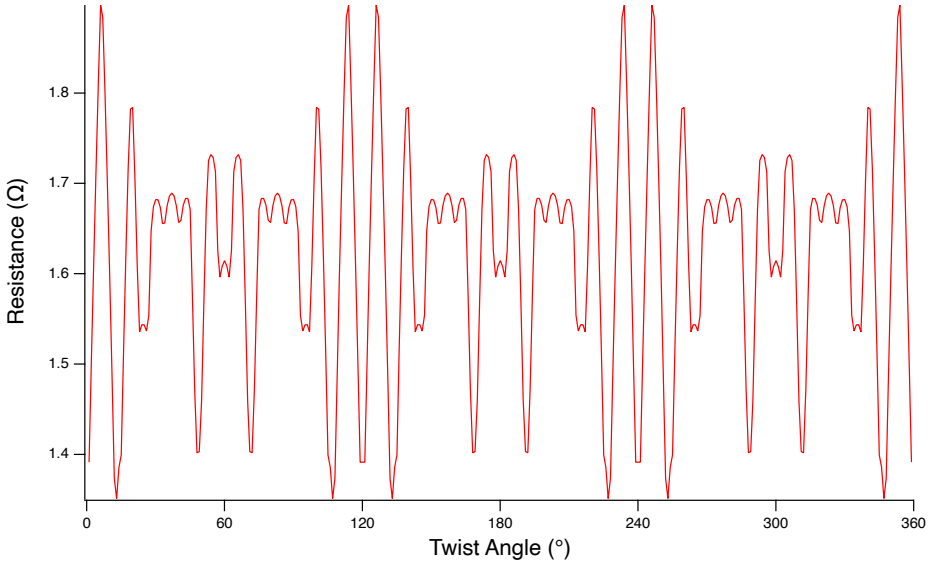

Figure 8: Resistance vs Angle graph of a hexagonal Moiré pattern with $R = 30$, $r = 15$

Table 1: Sample values from Fig. 8

$\theta(^\circ)$	$R_e(\Omega)$
1.0000	1.3913
2.0000	1.5036
3.0000	1.6104
4.0000	1.7133
5.0000	1.8095
6.0000	1.8974
7.0000	1.8838
8.0000	1.7973
9.0000	1.7003
10.0000	1.5979

Although the values within Table 1 are given *accurate* to 4 decimal places, the actual values were *precise* up to 15 decimal places, they are abbreviated here for brevity. Error bars are omitted from Fig. 8 because they are miniscule.

Computing the uncertainties of the obtained resistance values is intractable, due to the complexity of the computational process, including but not limited to hexagonal grid generation (trigonometric functions), rotation matrices (matrix-vector dot-products), line intersection algorithms, and finally, a linear system solver to perform nodal analysis.

The graph exhibits a few peculiarities, most notably, that it is symmetric across 6 lines of symmetry $\theta = [0^\circ, 60^\circ, 120^\circ, 180^\circ, 240^\circ, 300^\circ]$, this is because of the geometry of the hexagon shape, which itself has 6 lines of symmetry. Moreover, the graph reveals that the optimum angle for minimum resistance within this particular configuration ($R = 30$ and $r = 15$) is $13 \pm 1^\circ$ (the error is used due to the angle increment used) with resistance of $1.35 \pm 0.03\,\Omega$ (the uncertainty is calculated from the resistance difference between adjacent angles such as 14°) a far result from twisted bilayer graphene's superconductivity at the magic angle 1.1°.

As such, it can be concluded that twisted bilayer graphene's superconductivity cannot be explained using a circuit model of Moiré patterns, and rather, the phenomena is attributed to quantum interactions.

4 Evaluation

The computational method used within this investigation lends itself to many benefits. First of all, the required complex graphene manufacturing processes and equipment to sustain near absolute zero temperatures are completely sidestepped, making such an investigation viable for an IB student. Moreover, even if 3d-printed Moiré patterns are generated using a conductive filament, the simulation allows for virtually non-existent random errors which would not be possible in physical conditions due to the precision of computer hardware (≈ 15 decimal points). Error sources such as irreproducible contact surfaces with an Ohmmeter and uneven filament thickness are completely avoided.

Several computational complexity problems had to be overcome during the programming of the simulation. A grid-based intersection algorithm was used to exploit the limited length of each segment within the Moiré lattice (i.e., 1), reducing the time complexity of node generation from $\mathcal{O}(n \log n)$ to $\mathcal{O}(n)$ (e.g., the time required to calculate all intersections between 10 segments is approximately proportional to 10 s instead of $10 \log 10$ s). Also, duplicate nodes had to be removed (e.g., there are 3 nodes exactly at the center of the lattice $(0, 0)$ due to the 3 ($\curlywedge$) segments) because they invalidate the matrix $\mathbf{G}$ with infinite conductances (0 resistance). Finally, a sparse matrix solver was used to solve Eq. 4 (because most $\mathbf{G}_{i,j} = 0\,\Omega^{-1}$) reducing both the complexity and memory requirements of QR-decomposition.[5] As a result of these optimizations, calculating the effective resistance of the Moiré lattice (with $R = 30$, $r = 15$) for a single twisting angle took merely ≈ 30 s. Calculating all the datapoints for Fig. 8 took ≈ 3 hours.

Yet, there are lots of improvements to be made regarding the research method. Within this experiment, it is assumed that there is no interlayer resistance between the twisted bilayer graphene sheets. This does not resemble graphene, where π-bonds are formed, enabling *intralayer* and not *interlayer* conductivity. As such, an additional interlayer resistance should be implemented when nodes are generated to accurately mirror the physics of graphene atoms.

Lastly, there are systematic errors due to the addition of the reference circle: the resistances in Fig. 8 are lower than they should be as the reference circle provides additional paths for electricity to flow through. As mentioned within Section 2.1, one way to combat this is to increase both R (resembling an infinite plane of graphene) and r, in order to minimize the systematic error caused by the reference circle. Measuring the effects R and r have on the resistance of the Moiré patterns would also be an interesting research direction.

5 Conclusion

In conclusion, twisted bilayer graphene's superconductivity cannot be explained through an Ohmic representation of Moiré patterns due to a significant deviation between the magic angle and the optimal twist angle computed (13°). As such, quantum mechanics modelling methods must be used instead in order to predict the characteristics of Moiré lattices. Previous work done by [6] does exactly that, it utilizes Density Functional Theory

and Electronic Band Structure calculations to propose potential 2d-layered materials with desirable properties, while successfully obtaining the superconducting magic angle of 1.1°.

However, it is yet to be known whether these quantum interactions can be modelled by simply using interlayer resistance between the graphene sheets. Further research is required, but this investigation has established the required preliminary work.

References

[1] Y. Cao, V. Fatemi, S. Fang, K. Watanabe, T. Taniguchi, E. Kaxiras, and P. Jarillo-Herrero, "Unconventional superconductivity in magic-angle graphene superlattices," *Nature*, vol. 556, no. 7699, pp. 43–50, 2018, ISSN: 1476-4687. DOI: 10.1038/nature26160. [Online]. Available: https://doi.org/10.1038/nature26160.

[2] S. Carr, D. Massatt, S. Fang, P. Cazeaux, M. Luskin, and E. Kaxiras, "Twistronics: Manipulating the electronic properties of two-dimensional layered structures through their twist angle," *Phys. Rev. B*, vol. 95, p. 075 420, 7 Feb. 2017. DOI: 10.1103/PhysRevB.95.075420. [Online]. Available: https://link.aps.org/doi/10.1103/PhysRevB.95.075420.

[3] L. W. Nagel and D. Pederson, "Spice (simulation program with integrated circuit emphasis)," EECS Department, University of California, Berkeley, Tech. Rep. UCB/ERL M382, Apr. 1973. [Online]. Available: http://www2.eecs.berkeley.edu/Pubs/TechRpts/1973/22871.html.

[4] E. Cheever, *Modified nodal analysis intro*. [Online]. Available: https://lpsa.swarthmore.edu/Systems/Electrical/mna/MNA2.html.

[5] NVIDIA, *Cusolver cuda toolkit documentation*. [Online]. Available: https://docs.nvidia.com/cuda/cusolver/index.html.

[6] G. A. Tritsaris, S. Carr, Z. Zhu, Y. Xie, S. B. Torrisi, J. Tang, M. Mattheakis, D. T. Larson, and E. Kaxiras, "Electronic structure calculations of twisted multi-layer graphene superlattices," *2D Materials*, vol. 7, no. 3, p. 035 028, Jun. 2020. DOI: 10.1088/2053-1583/ab8f62. [Online]. Available: https://doi.org/10.1088%2F2053-1583%2Fab8f62.